Detecting Interactions between the Renal Autoregulation Mechanisms in Time and Space

Christopher G. Scully*, *Member, IEEE*, Nicholas Mitrou, Branko Braam, Willliam A. Cupples, and Ki H. Chon, *Senior Member, IEEE*

Abstract—*Objective:* Our objective is to identify localized interactions between the renal autoregulation mechanisms over time. *Methods:* A time-varying phase-randomized wavelet bicoherence detector for quadratic phase coupling between tubuloglomerular feedback and the myogenic response is presented. Through simulations we show its ability to interrogate quadratic phase coupling. The method is applied to kidney blood flow and laser speckle imaging sequences of cortical perfusion from anesthetized rats before and after nonselective inhibition of nitric-oxide synthase. *Results:* Quadratic phase coupling in kidney blood flow data was present in four out of nine animals during the control period for 13.0 ± 5.6% (mean ± SD) of time and in five out of nine animals during inhibition of nitric-oxide synthase for 15.8 ± 8.2% of time. Approximately 60% of time-series extracted from laser speckle imaging pixels of the renal cortex showed significant quadratic phase coupling. Pixels with significant coupling had a median coupling length of 10.8 ± 2.2% and 12.1 ± 3.1% of time with the 95th percentile of pixels being coupled for 25.5 ± 4.4% and 30.9 ± 6.4% of time during control and inhibition of nitric-oxide synthase, respectively. *Conclusion:* These results indicate quadratic phase coupling exists in short time intervals between tubuloglomerular feedback and the myogenic response and is detected more often in local renal perfusion signals than whole kidney blood flow in anesthetized rats. *Significance:* Combining the detector and laser speckle imaging provides identification of coordination between renal autoregulation mechanisms that is localized in time and space.

Index Terms—Bispectrum, laser speckle contrast imaging (LSCI), quadratic phase coupling (QPC), renal autoregulation.

*C. G. Scully was with the Department of Biomedical Engineering, Worcester Polytechnic Institute, Worcester, MA 01609 USA, and is currently with the Office of Science and Engineering Laboratories, Center for Devices and Radiological Health, US Food and Drug Administration, Silver Spring, MD 20993 USA (e-mail: christopher.scully@fda.hhs.gov).

N. Mitrou and W. A. Cupples are with the Department of Biomedical Physiology and Kinesiology, Simon Fraser University.

B. Braam is with the Department of Medicine and Physiology, University of Alberta.

K. H. Chon is with the Department of Biomedical Engineering, University of Connecticut.

I. INTRODUCTION

HIGHER-ORDER spectral analysis can provide insight into the nonlinear interactions between physiological systems. In physiological systems, nonlinear interactions between feedback mechanisms may include one system modulating the amplitude or frequency of another [1]. Amplitude modulation results in two sinusoids generating a third with a frequency at $f_1 + f_2$ and a phase equal to $\varphi_1 + \varphi_2$. This phase relationship defines the interaction between components 1 and 2 as quadratic phase coupling (QPC). Frequency modulation of one signal by another will also result in a frequency at $f_1 + f_2$ but without the phase equal to $\varphi_1 + \varphi_2$, and this is defined as quadratic frequency coupling (QFC). QPC implies QFC, but QFC can occur without QPC [2].

Renal autoregulation contains at least two mechanisms that operate to attenuate blood pressure fluctuations in nephrons (the functional unit of the kidney) [3]. Both mechanisms oscillate within frequency regions identified from single nephron laser Doppler recordings: tubuloglomerular feedback (TGF) operates within a frequency range of 0.02–0.06 Hz and the myogenic response operates within a frequency range of 0.1–0.3 Hz in anesthetized rats [4]. The two mechanisms act to constrict and dilate the afferent arteriole preceding each nephron producing an inherent TGF–myogenic interaction [5] that has been shown by Volterra–Wiener analysis of whole kidney blood flow to be nonlinear [6]. Wavelet analysis of single nephron laser Doppler signals showed that TGF modulates the amplitude and frequency of the myogenic response [7]–[9]. TGF control over the myogenic response represents coordination between the two mechanisms [8].

Using a time-invariant bispectrum detector, the TGF–myogenic interaction was identified in tubule pressure signals for normotensive rats as QPC but not in spontaneously hypertensive rats [10]. The lack of detection in spontaneously hypertensive rats was believed to be caused by their time-varying dynamics resulting in the interaction occurring over time instances shorter than what could be detected [10]. A time-varying bispectrum detector was developed and applied to renal autoregulation to identify QFC but could not discriminate QPC [2]. The results showed that periods of QFC could be detected in tubule pressure as well as whole kidney blood flow in normotensive and hypertensive rats [2]. Since the study only tested for QFC, it could not be determined if the nonlinear interaction was only QFC, which could be frequency modulation, or also may

have included QPC, which could represent amplitude modulation. Interactions occurring at the individual nephron level will be filtered out in whole kidney blood flow recordings [10].

Therefore, differentiating QFC and QPC in renal autoregulation is restricted by the acquisition of signals related to flow in a limited number of nephrons as well as the time-varying nature of renal autoregulation dynamics. Time-varying detectors have been proposed that provide short-time QPC detection [11]–[14]. Laser speckle imaging can monitor perfusion across the renal cortex simultaneously to acquire signals related to the dynamics of local flow changes [15]–[17].

It is important to understand autoregulation in depth because of its unique role in protecting renal structure and stabilizing renal function. Hypertension is the single most important cause of renal disease leading to dialysis and transplantation [18] and autoregulation mediated by the myogenic and TGF mechanisms is the only regulator of kidney blood flow that responds appropriately to blood pressure changes, adjusting pre-glomerular resistance to protect the glomerular capillaries and to stabilize renal function [3]. Weakness of autoregulation is well known to predispose to glomerular damage and renal failure [19], [20].

In this study a wavelet bicoherence (WBIC) detection procedure is modified and applied to laser speckle contrast imaging (LSCI) sequences of the renal cortex to detect locations with QPC between the TGF and myogenic mechanisms over short time periods. The statistical properties of the detector and ability to discriminate between amplitude and frequency modulation are shown using simulations. The method is applied to whole kidney blood flow signals and LSCI to identify QPC at locations across the renal surface.

II. QUADRATIC PHASE COUPLING DETECTOR

The time-invariant bispectrum can be estimated by the expected value of the triple Fourier transform ($X(f)$) product over K segments (1), where $*$ represents the complex conjugate

$$\mathrm{BS}\,(f1, f2) = E\,[X\,(f_1)\,X\,(f_2)\,X^*\,(f_1 + f_2)]. \quad (1)$$

The bicoherence is a normalized version of the bispectrum with values from 0 to 1 and is estimated over K segments

$$|\mathrm{BIC}\,(f1, f2)\,| = \frac{|\mathrm{BS}\,(f_1, f_2)|}{\sqrt{E\left[|X\,(f_1)\,X\,(f_2)|^2\right] E\left[|X\,(f_1 + f_2)|^2\right]}}. \quad (2)$$

The magnitude of the bicoherence is often used as a detector for QPC with a 95% significance level of zero bicoherence, defined by Elgar and Guza as $\sqrt{(6/2K)}$, where K is the number of segments [21], [22]. It has been shown that the bicoherence alone is not an appropriate indicator of QPC if the phases are not randomized across segments, as QFC without phase coupling will provide high bicoherence levels given constant phase relationships [13], [23]. Fackrell and McLaughlin showed that combination of the bicoherence and biphase statistical tests can discriminate cases of QPC [24]. QPC can be declared when the biphase is close to 0 across segments and the bicoherence is high. Usually at least eight segments of equal data length are required to make a designation of QPC, so that relatively long data lengths are necessary. For this reason, time-varying bispectral

detectors have been developed [14] and investigated, including those based on wavelet analysis [13].

The time-varying wavelet spectrum is defined as (3), where $x(t)$ represents the signal and ψ represents the wavelet function that is shifted throughout time and dilated at scales, s, to generate a spectral estimate across time and scales

$$w\,(s, t) = \frac{1}{\sqrt{s}} \int_{-\infty}^{\infty} x\,(\tau)\,\psi^*\left(\frac{\tau - t}{s}\right) d\tau. \quad (3)$$

The frequency of the wavelet spectrum is related to $1/s$. We use a Morlet wavelet with natural frequency of 6. Just as the time-invariant bispectrum can be determined by the expected value of the triple product of the Fourier transform in (1) over K segments, the wavelet bispectrum can be estimated at each time point by the integral of the wavelet spectrum as

$$\mathrm{WB}\,(f_1, f_2, n) = \int_{n-T/2}^{n+T/2} w\,(f_1, \tau)\,w\,(f_2, \tau)\,w^*\,(f_1 + f_2, \tau)\,d\tau. \quad (4)$$

An integration time T is selected to estimate the wavelet bispectrum at each time location. Equivalent to (2), the WBIC can then be estimated as

$$|\mathrm{WBIC}\,(f_1, f_2, n)| =$$
$$\frac{|\mathrm{WB}(f_1, f_2, n)|}{\sqrt{\int_{n-T/2}^{n+T/2} |w\,(f_1, \tau)\,w(f_2, \tau)|^2\,d\tau \int_{n-T/2}^{n+T/2} |w\,(f_1 + f_2, \tau)|^2\,d\tau}}. \quad (5)$$

The WBIC will be close to 1 when there is wavelet power at f_1, f_2, and f_{1+2} and the biphase at (f_1, f_2) is constant across the integration time. This can be used to define QFC. QPC requires a biphase ($\varphi_1 + \varphi_2 - \varphi_3$) of 0.

Kim *et al.* proposed a procedure to randomize the biphase when estimating the time-invariant bicoherence by multiplying the biphase by a random variable, R, at each segment [23]. When the biphase is close to 0, as in the case of QPC, multiplying the biphase at each segment by a random variable will still keep the biphase close to 0 so that a high bicoherence will result. When the biphase is not close to 0 but constant across the segments, the biphase will be randomized across segments when multiplied by the random variable resulting in a reduced bicoherence estimate. Li *et al.* applied this approach to time-varying wavelet analysis to develop the phase-randomized wavelet bispectrum (WBPR)

$$\mathrm{WBPR}\,(f_1, f_2, n) = \int_{n-T/2}^{n+T/2} |w\,(f_1, \tau)\,w\,(f_2, \tau)\,w^*\,(f_1$$
$$+ f_2, \tau)\,|e^{iR(\tau)\varphi_d(f_1, f_2, \tau)}\,d\tau. \quad (6)$$

φ_d represents the estimated biphase, and R the random variable at each time point multiplied by the biphase [13]. The phase-randomized wavelet bicoherence (WBICPR) is estimated as

$$|\mathrm{WBICPR}\,(f_1, f_2, n)| =$$
$$\frac{|\mathrm{WBPR}(f_1, f_2, n)|}{\sqrt{\int_{n-T/2}^{n+T/2} |w\,(f_1, \tau)\,w(f_2, \tau)|^2\,d\tau \int_{n-T/2}^{n+T/2} |w\,(f_1 + f_2, \tau)|^2\,d\tau}}. \quad (7)$$

TABLE I
PROCEDURE TO DETECT TIME-VARYING QUADRATIC PHASE COUPLING
BETWEEN THE RENAL AUTOREGULATION MECHANISMS

1	Estimate the wavelet spectrum and identify the maximum amplitude and corresponding frequency across the two frequency ranges: $f_1 = [0.02 - 0.06]$ and $f_2 = [0.1 - 0.3]$ Hz (3)
2	Extract the wavelet coefficients $w(f_1, t)$ and $w(f_2, t)$
3	Compute the WBIC and biphase at $(f_1, f_2\ t)$ with an integration time of 100 s (5)
4	Compute the WBICPR at $(f_1, f_2\ t)$ (7)
5	Compute K WBICPR surrogates (8) and use the mean plus two standard deviations at each time point to estimate the QPC threshold
6	Compare the WBICPR with the threshold to determine times with QPC

To determine the significance of the WBICPR, Li *et al.* proposed a surrogate data approach by adding a random variable to the biphase prior to multiplying it by the random integer R [13]. This has the intended effect of shifting the biphase away from 0 when QPC is present, so that when the phase-randomization procedure is applied the resultant bicoherence values represent the statistical signature of the absence of QPC. However, adding a random variable to the biphase can sometimes shift the biphase towards 0 when it is not close to it, creating a bimodal distribution when generating multiple trials from surrogate data. We only want to determine the expected phase-randomized bicoherence when the biphase is away from 0 to determine a threshold. In this study, the biphase at each time point is replaced with a uniform random variable θ that is U$[-\pi : -1, 1 : \pi]$. The wavelet bispectrum for each surrogate trial is then

$$\text{WB}surr(f_1, f_2, n) = \int_{n-T/2}^{n+T/2} |w(f_1, \tau) w(f_2, \tau)$$
$$\times w^*(f_1 + f_2, \tau)| e^{i\theta(\tau)} d\tau. \quad (8)$$

The phase-randomized bicoherence estimate is determined for K realizations of θ, and the mean plus 2 standard deviations at each time point is used as a threshold. This procedure provides the expected WBICPR given the signal dynamics without QPC.

WBIC, WBICPR, and surrogate-derived thresholds are computed by first tracking the low and high dominant frequencies, f_1 and f_2, in the wavelet spectrum as the frequency corresponding to the maximum amplitude at each time point within that range. f_1 represents the TGF component (0.02–0.06) Hz and f_2 the myogenic component (0.1–0.3). Amplitude and frequency modulation operations will result in sum and difference frequencies in the power spectrum at $(f_1 + f_2)$ and $(f_1 - f_2)$, and a bispectrum peak at (f_1, f_2). WBIC values are tracked at the (f_1, f_2) pair across time to look for QPC between the TGF and myogenic mechanisms. Results are computed at this frequency pair as it varies over time for the designation of a nonlinear interaction between the two mechanisms. Table I summarizes the detection procedure.

III. MATERIALS AND METHODS

A. Detection Properties Simulation

Equation (9) represents signals with and without QPC, a condition set by varying the properties of the third sinusoid

$$sig(t) = A_1 \sin(2\pi f_1 t + \varphi_1) + A_2 \sin(2\pi f_2 t + \varphi_2)$$

$$+ A_3 \sin(2\pi f_3 t + \varphi_3) + r(t). \quad (9)$$

The test signal consists of three sinusoids with added white Gaussian noise, r. f_1 was set to 0.03 Hz and f_2 to 0.13 Hz, representative of the TGF and myogenic renal autoregulation components, respectively, with phases φ_1 and φ_2 set as uniform random variables U$[-\pi, \pi]$. The frequency of the third sinusoid, f_3, was set to the sum of the first two, 0.16 Hz, to represent frequency coupling, and QPC was set by making φ_3 equal to $\varphi_1 + \varphi_2$ so that the biphase $(\varphi_1 + \varphi_2 - \varphi_3)$ is equal to 0. Otherwise, when QPC was not present φ_3 was set as a uniform random variable U$[-\pi, \pi]$. A_1 and A_2 were set to 1, and A_3 was varied to represent the coupling strength.

Thirty signal sections, alternating with and without QPC, were concatenated together to generate signals with the time-varying presence of QPC. Section lengths were varied from [64, 128, 256, 512, 1024] s. Signals at each length were generated with coupling amplitudes, A_3, varied from [0, 0.25 0.5, 0.75, 1.0].

The WBICPR was computed for each concatenated signal and coupling amplitude at (f_1, f_2, t). True positives were declared when the phase-randomized bicoherence was greater than the surrogate-derived threshold when QPC was present. True negatives were declared when the phase-randomized bicoherence was not greater than the threshold during periods when QPC was not present.

B. Amplitude and Frequency Modulation Simulation

This test is designed to determine if the proposed algorithm is able to specifically detect QPC (represented by amplitude modulation) and not QFC (represented by frequency modulation). Four signals (10–13) were developed to represent the following cases: Case 1: two independent signals without amplitude or frequency modulation; Case 2: the higher frequency sinusoid, f_2, is amplitude modulated by the lower, f_1; Case 3: f_2 is frequency modulated by f_1; and Case 4: v is both amplitude and frequency modulated by f_1

$$\text{Case1}(t) = \sin(2\pi f_1 t + \varphi_1) + \sin(2\pi f_2 t + \varphi_2) + r(t) \quad (10)$$

$$\text{Case2}(t) = (1 + \sin(2\pi f_1 t + \varphi_1)) * \sin(2\pi f_2 t + \varphi_2) + r(t) \quad (11)$$

$$\text{Case3}(t) = \sin\left(2\pi f_2 t + 2\pi * f_1 * \int_0^t \sin(2\pi f_1 \tau)\, d\tau\right) + r(t) \quad (12)$$

$$\text{Case4}(t) = \left(\int_0^t 1 + \sin(2\pi f_1 t + \varphi_1)\right) * \sin\left(\int_0^t 2\pi f_2 t + 2\pi\right.$$
$$\left. * f_1 * \int_0^t \sin(2\pi f_1 \tau)\, d\tau\right) + r(t). \quad (13)$$

One hundred trials of each case were generated with random Gaussian white noise, r, and signal length of 1500 s. f_1 was set to 0.03 Hz and f_2 to 0.13 Hz to represent the TGF and myogenic mechanisms, respectively. The amount of time the phase-randomized bicoherence was above the significance threshold was determined for each trial and the mean and stan-

dard deviation were computed over all trials. The number of trials with significant time-invariant bicoherence, biphase, and QPC was also determined using the statistical tests proposed for each case [21], [22], [24].

C. Experimental Data Collection

Data were used from a previously published report that probed a different question [25]. All experiments were approved by the Animal Care Committee of Simon Fraser University, in accordance with the guidelines of the Canadian Council of Animal Care. Male Long-Evans rats (Harlan, Livermore, CA, USA) ($N = 9$), aged 10–14 weeks were used. Anesthesia was induced with 4% isoflurane in inspired gas (30% O_2, 70% air, 750 mL/min) and reduced to 2% thereafter. The trachea was cannulated and animals ventilated by a small animal respirator (TOPO, Kent Scientific, Torrington, CT, USA) adjusted to match the natural breathing rate of each animal ($\sim$45 breaths per minute). The left femoral vein was cannulated (PE-50) for infusion of saline containing 2% bovine serum albumin (1% body weight per hour). A subcostal flank incision exposed the left kidney. Once freed from surrounding fat, the kidney was mounted in a plastic cup anchored to the table. Stopcock grease (Dow Corning, Midland, MI, USA) was placed in the cup to prevent motion and position the kidney towards the LSCI camera. The renal artery was stripped of fat and renal nerves. A transit time ultrasound flow probe (TS420, Transonic Systems, Ithaca, NY, USA) was mounted on the renal artery to record whole kidney blood flow, secured with acoustic coupling gel (Surgilube and Nalco 1181). Blood pressure and kidney blood flow were recorded at 500 Hz. There was a 1-h postsurgery equilibration period.

LSCI was performed with the moorFLPI imaging system (Moor Instruments, Axminster, UK) using an exposure time of 2 ms and flux computed over a spatial set of pixels (113×152 pixels at 25 Hz sampling rate). An $\sim$4 mm hair was placed on the surface of the kidney, and the moorFLPI was positioned to capture the full hair in the viewing window resulting in the lens $\sim$20 cm from the surface. Data were recorded in each animal under spontaneous blood pressure during control conditions and non-selective nitric oxide synthesis (NOS) inhibition with intravenous infusion of N^{ω}-nitro-l-arginine methyl ester (L-NAME) (Sigma-Aldrich, Oakville, ON, Canada) at 10 mg/kg$_{\mathrm{BW}}$. Each recording period was 25 min in length.

A Gaussian spatial filter was applied to each frame to increase the signal-to-noise ratio [16]. The image series were down sampled by a factor of 4 and the time-series from each pixel location were low-pass filtered to 0.5 Hz and down sampled to 1 Hz to remove potential baroreflex, respiration, and cardiac components at higher frequencies [16]. Whole kidney blood flow data were low-pass filtered to 0.5 Hz and down sampled to 1 Hz. Whole kidney blood flow and the time-series extracted from each pixel of the filtered image series were tested for the presence of QPC.

IV. SIMULATION RESULTS

A. Statistical Properties of Detector

The concatenated test signals contain segments from (9) alternating with or without QPC. Fig. 1 illustrates our approach by comparing the power spectrum and WBIC results for a signal section with (top row) $\varphi_3 = \varphi_1 + \varphi_2$ to represent QPC and (bottom row) $\varphi_3 = U[-\pi, \pi]$. Fig. 1(a) and (e) shows the power spectra for the two scenarios. Three spectral peaks can be identified at the low frequency ($f_1 = 0.03$ Hz), high frequency ($f_2 = 0.13$ Hz), and sum of the low and high frequencies ($f_3 = 0.16$ Hz) in both spectra. No difference between the two segments can be discerned from the power spectra because phase relationships are suppressed. Fig. 1(b) represents the WBIC spectrum at the time point with QPC and Fig. 1(f) represents the same for a time point without QPC. In both cases, the WBIC is high in the area (0.03, 0.13) Hz and it is clear that this peak alone cannot discriminate between the two cases. Fig. 1(c) shows the absolute value of the wavelet biphase during QPC at the same time point as Fig. 1(b). In this case, the biphase is close to 0 around (0.03, 0.13) Hz as expected. In Fig. 1(g), the absolute value of the wavelet biphase is shown for the time point without QPC and is not close to 0. The wavelet biphase can discriminate between periods with and without QPC, but since the phases are constant across the integration time the bicoherence is high regardless of the state of QPC.

The phase-randomized bicoherence (7) during the two time points with and without QPC are shown in Fig. 1(d) and (h), respectively. When QPC is present the phase randomized bicoherence produces a high value in the area of (0.03, 0.13) Hz, Fig. 1(d), but when the phases are not coupled there is no peak in the area of (0.03, 0.13) Hz, Fig. 1(h). Multiplying the biphase at each time point by a random variable has little impact when the biphase is close to 0, so the bicoherence estimate remains high. When the biphase is constant but not close to 0, such as can happen in QFC, the random variable distorts biphase values so they are no longer constant across integration times.

The utility of the phase randomization procedure is further illustrated in Fig. 2. Here, signal segments with and without QPC ranging in size from 2048 to 64 data points from (9) were concatenated together. The true state of set QPC at each time point is shown by the dashed gray line in Fig. 2(c). Fig. 2(a) shows the WBIC (solid black line), phase-randomized bicoherence (solid gray line) and surrogate-derived threshold (dashed gray line) tracked at (0.03, 0.13) Hz across time. WBIC remains high across signal lengths since the frequency coupled component is always present, Eq. (9). The phase-randomized bicoherence is only high when biphase is close to 0, which occurs during periods with QPC. By comparing the phase-randomized bicoherence with surrogate-derived threshold, accurate detection of time points with QPC can be made for short data lengths as seen by the QPC decision in Fig. 2(c) (black line).

QPC detection was performed on the test signals described in Section III-A. Accuracy, sensitivity (rate of QPC detection when present), and specificity (rate of not detecting QPC when not present) as a function of the segment lengths and coupling amplitudes are shown in Fig. 3(a)–(c), respectively, at an integration time of 100 s using 40 surrogate trials. Sensitivity increases with increasing coupling amplitudes and segment lengths. At a coupling amplitude of 0 QPC is rarely detected. In this scenario, the third frequency is not present so we do not expect to detect QPC. Specificity remains at $\sim$85% across data lengths and coupling amplitudes. When the phase of the third frequency
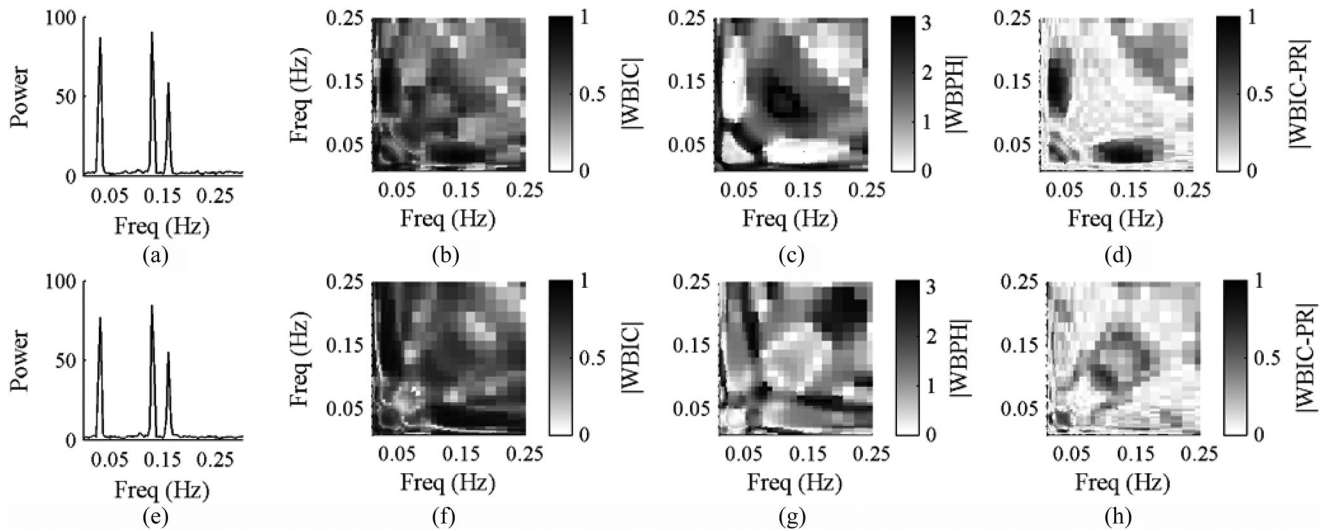
Fig. 1.   (a, e) Power spectral densities for the test signal in (9) for the case of quadratic phase coupling ($\varphi_3 = \varphi_1 + \varphi_2$) and without quadratic phase coupling ($\varphi_3 = U[-\pi, \pi]$). (b) WBIC for the test signal at a time when quadratic phase coupling is present. (c) Absolute value of the wavelet biphase at the same time point; note the phase is nearly zero at ($f_1 = 0.03$, $f_2 = 0.13$). (d) WBICPR when quadratic phase coupling is present; note the bicoherence values are nearly 1 at ($f_1 = 0.03$, $f_2 = 0.13$). (f) WBIC, (g) biphase, and (h) WBICPR at a time point without quadratic phase coupling.
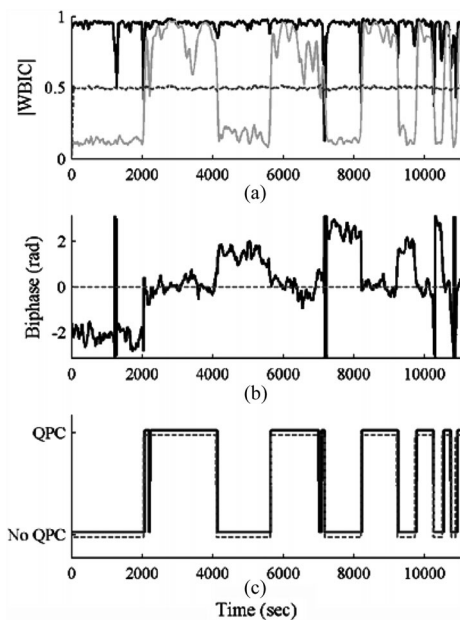
Fig. 2.   WBIC results at (f_1, f_2) over time for test signal with alternating periods with or with the presence of quadratic phase coupling. (a) WBIC (black line), WBICPR (light gray line) and surrogate data threshold (dashed gray line). (b) Wavelet biphase at (f_1, f_2). The true state of quadratic phase coupling is shown by the dashed gray line in (c), and the declared state based on the phase randomized surrogate data test is shown by the black line.

component is set as a random variable, we expect it to equal the sum of the first two components on occasion which results in true negatives being detected.

B. Distinguishing Amplitude Modulation

WBIC at (f_1, f_2) results for the 4 amplitude and frequency modulation cases (10–13) are shown in Fig. 4(a)–(c) for $K = 100$
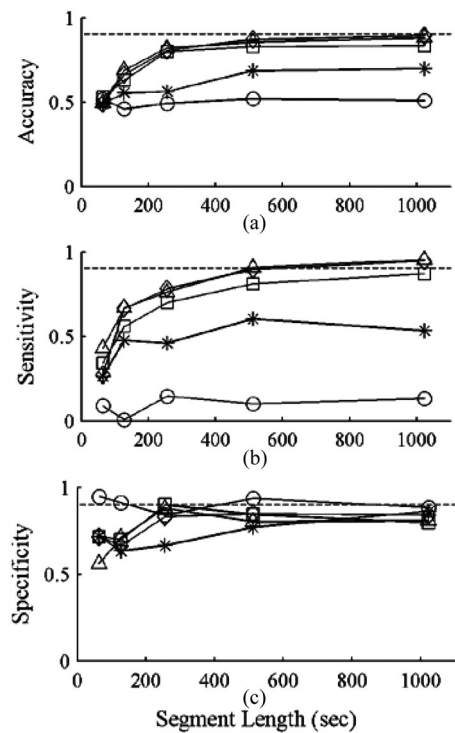
Fig. 3.   (a) Accuracy, (b) sensitivity, and (c) specificity for varying segment lengths and coupling amplitudes at an integration time of 100 s and 40 surrogate trials. Lines on each plot represent the amplitude of the third frequency component (circle 0.0, star 0.25, square 0.5, diamond 0.75, triangle 1.0). Dashed lines are at 0.9 for reference.

trials. WBIC is present during all four cases; however wavelet biphase is high for Cases 1 (no amplitude or frequency modulation) and 3 (only frequency modulation). In Cases 2 (only amplitude modulation) and 4 (amplitude and frequency modulation), the WBIC is increased and the wavelet biphase is close
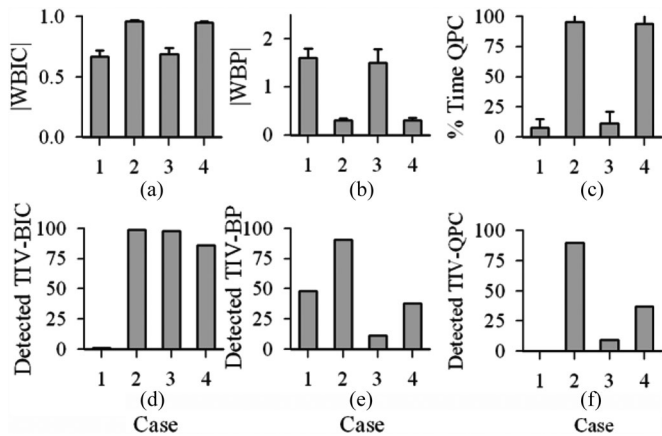
Fig. 4. Top row shows results from time-varying detector including (a) WBIC, (b) biphase, (c) and the percent of time QPC was detected for 100 trials (mean ± SD) for the four cases of amplitude and frequency modulation ((10)–(13)). Bottom row contains the time-invariant bicoherence detection results over the 100 trials: number of trials with significant (d) bicoherence, (e) biphase, and (f) quadratic phase coupling (significant bicoherence and biphase both detected).

to 0. QPC is consistently detected during Cases 2 and 4 (which include amplitude modulation) but not Case 3 (only frequency modulation). This demonstrates that the time-varying detector is able to differentiate amplitude and frequency modulation.

The number of trials with significant time-invariant bicoherence, biphase, and QPC are shown in Fig. 4(d)–(f) using the test described by Fackrell and McLaughlin [24]. High time-invariant bicoherence is present for the three cases with modulation. The time-invariant test detects amplitude modulation when it is present by itself in ~80% of the Case 2 trials, but QPC in Case 4 is only identified in ~5% of the trials even though it is present alongside frequency modulation. The WBICPR test detected QPC, when amplitude modulation alone was present (Case 2) and when amplitude and frequency modulation were simultaneously present (Case 4). This simulation provides an example of improved detection of QPC in the form of amplitude modulation using the WBIC technique, whether or not frequency modulation is also present.

V. EXPERIMENTAL RESULTS

A. Whole Kidney Blood Flow

A representative whole kidney blood flow recording for one animal after bolus infusion of L-NAME is shown in Fig. 5(a) with accompanying power spectrum in Fig. 5(c). A weak TGF signal component can be seen as a low frequency component relative to the strong myogenic signal between 0.1 and 0.3 Hz. Fig. 5(b) shows the tracked WBIC and WBICPR with its corresponding surrogate-derived threshold. The WBIC is high throughout most of the recording, but the phase-randomized bicoherence is only higher than the threshold for short time periods, when the light gray line (phase-randomized bicoherence) crosses the dark dashed gray line (threshold). This indicates the presence of transient QPC.

QPC was detected for at least a 100 s segment (the integration time) in whole kidney blood flow for 4 out of the 9 animals
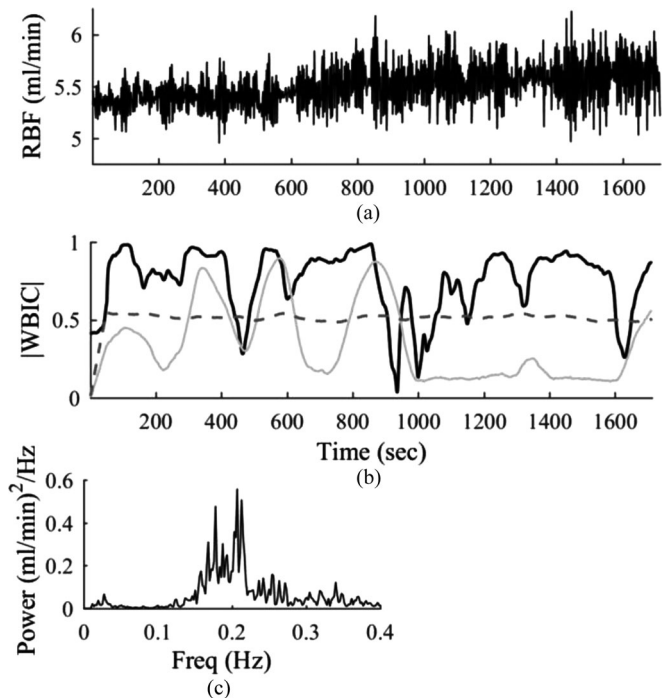
Fig. 5. (a) Whole kidney blood flow signal after bolus infusion of L-NAME for a single experiment. (b) WBIC (black line), WBICPR (solid light gray line), and surrogate-derived threshold (dashed gray line) tracked at (f_{TGF}, f_{MYO}, t). (c) Power spectrum of the whole kidney blood flow signal showing frequency content in the expected myogenic range, 0.1–0.3 Hz, and weak frequency content in the TGF range, ~0.02 Hz.

during the control period. In these four animals, QPC was present for $13.0 \pm 5.6\%$ (mean $\pm$ SD) of the signal recording length. After bolus infusion of L-NAME, QPC was present in five out of the nine animals for $15.8 \pm 8.2\%$ of the signal recording length.

B. Quadratic Phase Coupling Across the Renal Surface

Whole kidney blood flow signal contains dynamics averaged over all the nephrons in the kidney. This will attenuate dynamics from any one nephron that may display QPC. To test if localized QPC could be detected, the WBIC analysis was applied to time-series extracted from each filtered pixel.

Two pixel locations were selected from one animal's control and L-NAME periods to demonstrate QPC monitoring on a pixel-by-pixel basis. Fig. 6(a) and (b) shows the power spectra of the two locations during control and L-NAME periods, respectively. The myogenic response during L-NAME includes multiple peaks around 0.2 Hz. Fig. 6(c) shows the WBICPR for each of the two locations during control with the detection of when QPC is present. Limited, short-time periods with QPC exist for both locations. During L-NAME, QPC is present through much of the experimental recording at each location, Fig. 6(d), but timing of QPC is not consistent between locations.

Time-averaged WBICPR during control and L-NAME periods for one animal (same as Fig. 6) at each pixel location are shown in Fig. 7(a) and (b), respectively. During control, the WBICPR is low across the surface but during L-NAME it
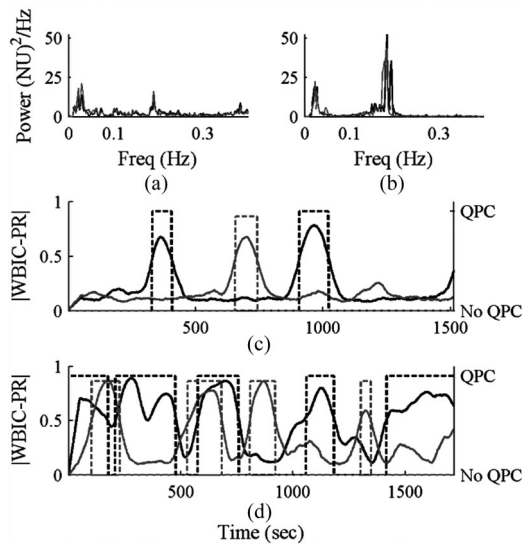
Fig. 6. Power spectra during the (a) control and (b) L-NAME period are shown for one animal at two locations. (c) WBICPR at the two locations during the control monitoring period with dashed lines representing the decision of QPC. (d) Same as (c) for the L-NAME monitoring period.
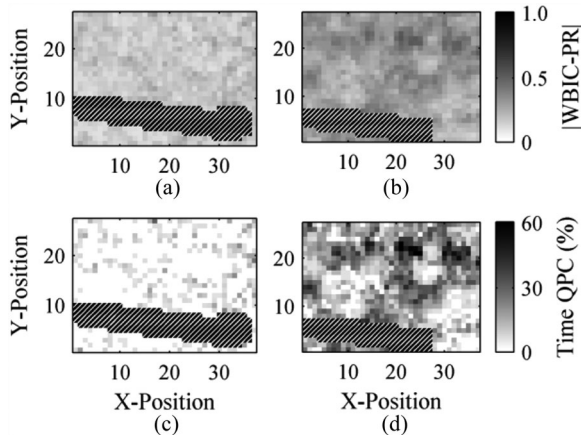
Fig. 7. (a) Time-averaged WBICPR during control and (b) L-NAME at each pixel location for the same animal as in Fig. 6. The percentage of time that WBICPR is greater than the surrogate-derived threshold at each pixel location after removal of segments less than 100 s during (c) control and (d) L-NAME. The black region with white lines represents the hair placed across the renal surface.

increases. The percentage of time that QPC was declared significant is shown in Fig. 7(c) and (d) for the control and L-NAME periods, after removal of segments less than the integration time, at each pixel location. During control periods, there is a sparse distribution of pixels with limited QPC. After bolus L-NAME infusion, much of the surface shows significant QPC with some locations showing QPC up to 60% of the time.

Over the nine experiments, time-series extracted from individual pixels generally depict limited QPC ($<20\%$), but in most experiments a portion of the pixels depict significantly more QPC, up to 40–60%. These locations with high amounts of QPC represent localized areas with myogenic and TGF mechanisms operating together. Table II quantifies the number of pixels with

TABLE II
QUADRATIC PHASE COUPLING DETECTED ACROSS THE RENAL SURFACE

	Control	L-NAME
Pixels with QPC (%)	57.7 ± 20.1	63.1 ± 14.1
Median of % Time QPC	10.8 ± 2.2	12.1 ± 3.1
95th Percentile of % Time QPC	25.5 ± 4.4	30.9 ± 6.4

Percentage of times that QPC is significant is only for pixels with significant QPC. Mean $\pm$ SD. $N = 9$.

significant QPC, and the amount of time that those pixels are coupled for. Approximately 60% of pixels have at least a 100 s period with QPC.

VI. DISCUSSION

We have developed an approach to detect time-varying QPC across the renal cortex. This can be used to discriminate between interactions that may cause QFC but not QPC (e.g., frequency modulation). In renal autoregulation, both amplitude and frequency modulation are part of the TGF–myogenic interaction [8], [9], [26]. The TGF–myogenic interaction is caused by both mechanisms affecting afferent arteriole resistance [5]. Interactions between the mechanisms allows TGF, which senses tubular fluid composition related to renal function, to help stabilize the faster myogenic mechanism, which senses a variable related to systemic pressure [27], to produce efficient renal autoregulation [5]. Discriminating between amplitude and frequency modulation allows interpretation of the physical mechanisms involved in the interaction. Amplitude modulation may be interpreted as TGF modifying the magnitude of changes in vessel diameter while frequency modulation describes how TGF alters the rate at which the myogenic response occurs. Combining the presented detector with laser speckle imaging allows study of the regional differences in the interactions between the mechanisms to improve our understanding of the physiological changes that occur during disease resulting in poorly functioning renal autoregulation.

Previously, a time-varying bispectrum procedure was described that used surrogate data to provide a significant threshold [2]. This approach only considered the bispectrum magnitude and could therefore not distinguish between QFC and QPC. The phase randomization procedure is computationally efficient compared to other surrogate data techniques because it only requires adjusting phase information after estimation of the wavelet biphase. In this way, the wavelet transform and WBIC do not need to be recomputed for each surrogate data trial. We used a wavelet previously applied to renal autoregulation data [26] and an integration time optimized for our frequencies of interest. These parameters can be varied if investigating a system with faster or slower components.

We focused our physiological investigation specifically on the TGF–myogenic interaction and whether QPC representing amplitude modulation could be detected between these two components by tracking the frequencies at (f_{TGF}, f_{MYO}). Limited QPC ($\sim 15\%$ to 20% of the time) was identified in whole kidney

blood flow signal. Previously, QFC was identified in whole kidney blood flow [2]. This may indicate that the majority of QFC previously identified was representative of frequency modulation with only limited periods of amplitude modulation. Using double wavelet analysis Sosnovtseva *et al.* showed the myogenic frequency sequence to have a relatively sharp spectral peak around the expected frequency of TGF, while the amplitude modulation spectral peak was broad in normotensive rats [28]. These results suggest that myogenic amplitude modulation may have more time-variance than myogenic frequency modulation and that TGF may not be the only mechanism that modulates the amplitude of the myogenic response. Nonlinear interactions may occur between neighboring nephrons [17], [29] and with a reported low frequency mechanism ($\sim$0.01 Hz) [30]. Siu *et al.* identified the presence of amplitude modulation by a low frequency source that was not found to cause frequency modulation [30]. We also previously identified modulation in normotensive and hypertensive rats across frequency ranges that may indicate either TGF or a low frequency modulator in laser Doppler signals [26]. The proposed method could be applied to determine the presence of these other interactions in renal autoregulation by varying the frequency ranges of interest or looking at cross-bicoherence between locations in laser speckle imaging [31].

Signals extracted from single pixels of LSCI have the potential to show much higher amounts of QPC, up to 60% of the time for pixels from certain locations, than signals from whole kidney blood flow signals. Locations where high amounts of QPC are identified may represent signals from single nephrons where we are able to identify the TGF and myogenic fluctuations. It was previously shown using time-invariant analysis that interactions could be identified in tubule pressure signals and laser Doppler signals from single nephrons [10], [32]. The advantage of LSCI is that it allows us to investigate interactions at multiple locations across the renal surface. This allowed us to see two locations in Fig. 6(d) that both had high amounts of QPC, but the time points of when QPC occurred varied between locations. This suggests the mechanisms causing QPC are local and supports that it is more difficult to identify QPC in whole kidney blood flow as fluctuations are averaged across all nephrons.

VII. CONCLUSION

In the present study we have provided a method to identify QPC over short time instances and in spatial locations. A time-varying procedure to detect QPC using a WBICPR procedure was modified for detection of the TGF–myogenic interaction. The detection procedure was applied to renal perfusion data generated with laser speckle contrast imaging which provides information about the renal autoregulation dynamics across the imaged renal surface. Combined, the imaging and analytical procedures identify locations where both renal autoregulation mechanisms are interacting in the form of QPC. More specifically the presented procedure identifies locations in time and space where TGF is having a direct influence on the myogenic response. The combination of laser speckle imaging and our

analytical procedure could be used to study the heterogeneity of interactions across time and space in healthy and diseased models. We applied the approach to the study of the TGF–myogenic interaction, but the procedure itself is general and can be applied to study any system with multiple control systems suspected of nonlinear interactions.

REFERENCES

[1] Y. Zhong *et al.*, "Autonomic nervous nonlinear interactions lead to frequency modulation between low-and high-frequency bands of the heart rate variability spectrum," *Amer. J. Physiol.—Regulatory Integr. Comparative Physiol.*, vol. 293, pp. R1961–R1968, Nov. 2007.

[2] R. Raghavan *et al.*, "Interactions between TGF-dependent and myogenic oscillations in tubular pressure and whole kidney blood flow in both SDR and SHR," *Amer. J. Physiol.–Renal Physiol.*, vol. 290, pp. F720–F732, Mar. 2006.

[3] W. A. Cupples and B. Braam, "Assessment of renal autoregulation," *Amer. J. Physiol.—Renal Physiol.*, vol. 292, pp. F1105–F1123, Apr. 2007.

[4] K. P. Yip *et al.*, "Mechanisms of temporal variation in single-nephron blood flow in rats," *Amer. J. Physiol.—Renal Physiol.*, vol. 264, pp. F427–F434, Mar. 1993.

[5] W. A. Cupples, "Interactions contributing to kidney blood flow autoregulation," *Current Opinion Nephrology Hypertension*, vol. 16, pp. 39–45, Jan. 2007.

[6] K. H. Chon *et al.*, "Detection of interactions between myogenic and TGF mechanisms using nonlinear analysis," *Amer. J. Physiol.—Renal Physiol.*, vol. 267, pp. F160–F173, Jul. 1994.

[7] D. J. Marsh *et al.*, "Nonlinear interactions in renal blood flow regulation," *Amer. J. Physiol.—Regulatory Integr. Comparative Physiol.*, vol. 288, pp. R1143–R1159, May 2005.

[8] D. J. Marsh *et al.*, "Frequency encoding in renal blood flow regulation," *Amer. J. Physiol.—Regulatory Integr. Comparative Physiol.*, vol. 288, pp. R1160–R1167, May 2005.

[9] O. Sosnovtseva *et al.*, "Double-wavelet approach to study frequency and amplitude modulation in renal autoregulation," *Phys. Rev. E*, vol. 70, p. 031915, Sep. 2004.

[10] K. H. Chon *et al.*, "Interactions of TGF-dependent and myogenic oscillations in tubular pressure," *Amer. J. Physiol.—Renal Physiol.*, vol. 288, pp. F298–F307, Feb. 2005.

[11] J. Jamšek *et al.*, "Wavelet bispectral analysis for the study of interactions among oscillators whose basic frequencies are significantly time variable," *Phys. Rev. E*, vol. 76, p. 046221, Oct. 2007.

[12] B. P. Van Milligen *et al.*, "Wavelet bicoherence: A new turbulence analysis tool," *Phys. Plasmas*, vol. 2, p. 3017, Aug. 1995.

[13] X. Li *et al.*, "The comodulation measure of neuronal oscillations with general harmonic wavelet bicoherence and application to sleep analysis," *NeuroImage*, vol. 48, p. 501, Nov. 2009.

[14] J. Jamšek *et al.*, "Nonlinear cardio-respiratory interactions revealed by time-phase bispectral analysis," *Phys. Med. Biol.*, vol. 49, p. 4407, 2004.

[15] R. Bezemer *et al.*, "Real-time assessment of renal cortical microvascular perfusion heterogeneities using near-infrared laser speckle imaging," *Opt. Express*, vol. 18, pp. 15054–61, Jul. 5 2010.

[16] C. G. Scully *et al.*, "Detecting physiological systems with laser speckle perfusion imaging of the renal cortex," *Amer. J. Physiol.—Regulatory Integr. Comparative Physiol.*, vol. 304, pp. R929–R939, Jun. 2013.

[17] N.-H. Holstein-Rathlou *et al.*, "Nephron blood flow dynamics measured by laser speckle contrast imaging," *Amer. J. Physiol.—Renal Physiol.*, vol. 300, pp. F319–F329, Feb. 2011.

[18] R. Loutzenhiser *et al.*, "Renal autoregulation: new perspectives regarding the protective and regulatory roles of the underlying mechanisms," *Amer. J. Physiol.—Regulatory Integr. Comparative Physiol.*, vol. 290, pp. R1153–67, May 2006.

[19] A. K. Bidani *et al.*, "Renal autoregulation and vulnerability to hypertensive injury in remnant kidney," *Amer. J. Physiol.*, vol. 252, pp. F1003–10, Jun. 1987.

[20] S. J. Van Dijk *et al.*, "Interaction between Rf-1 and Rf-4 quantitative trait loci increases susceptibility to renal damage in double congenic rats," *Kidney Int.*, vol. 68, pp. 2462–72, Dec. 2005.

[21] S. Elgar and R. Guza, "Statistics of bicoherence," *IEEE Trans. Acoust., Speech, Signal Process.*, vol. 36, pp. 1667–1668, Oct. 1988.

[22] S. Elgar and G. Sebert, "Statistics of bicoherence and biphase," *J. Geophys. Res. C—Oceans*, vol. 94, pp. 10993–10998, Aug. 1989.

[23] T. Kim *et al.*, "A novel QPC detector for the health monitoring of rotating machines," in *Proc. IEEE Instrum. Meas. Technol. Conf.*, 2007, pp. 1–6.

[24] J. Fackrell and S. McLaughlin, "Quadratic phase coupling detection using higher order statistics," presented at the IEE Colloq. Higher Order Statist. Signal Process.: Are They of Any Use?, London, U.K., 1995.

[25] N. Mitrou *et al.*, "Laser speckle contrast imaging reveals large-scale synchronization of cortical autoregulation dynamics influenced by nitric oxide," *Amer. J. Physiol.—Renal Physiol.,* vol. 308, pp. F661–F670, Apr. 2015.

[26] C. G. Scully *et al.*, "Time–frequency approaches for the detection of interactions and temporal properties in renal autoregulation," *Ann. Biomed. Eng.*, vol. 41, pp. 172–184, Jan. 2013.

[27] R. Loutzenhiser *et al.*, "Systolic pressure and the myogenic response of the renal afferent arteriole," *Acta Physiol. Scand.*, vol. 181, pp. 407–13, Aug. 2004.

[28] O. Sosnovtseva *et al.*, "The effect of L-NAME on intra-and inter-nephron synchronization," *Eur. J. Pharmaceutical Sci.*, vol. 36, pp. 39–50, Jan. 2009.

[29] D. J. Marsh *et al.*, "Electrotonic vascular signal conduction and nephron synchronization," *Amer. J. Physiol.—Renal Physiol.*, vol. 296, pp. F751–F761, Apr. 2009.

[30] K. L. Siu *et al.*, "Detection of low-frequency oscillations in renal blood flow," *Amer. J. Physiol.—Renal Physiol.*, vol. 297, pp. F155–F162, Jul. 2009.

[31] K. L. Siu and K. H. Chon, "On the efficacy of the combined use of the cross-bicoherence with surrogate data technique to statistically quantify the presence of nonlinear interactions," *Ann. Biomed. Eng.*, vol. 37, pp. 1839–1848, Sep. 2009.

[32] K. L. Siu *et al.*, "Statistical approach to quantify the presence of phase coupling using the bispectrum," *IEEE Trans. Biomed. Eng.*, vol. 55, pp. 1512–1520, May 2008.

Authors' photographs and biographies not available at the time of publication.